- Technical Paper -

AN EXPERIMENTAL STUDY ON SHEAR CARRIED BY FIBERS OF FRC BEAMS WITH DIFFERENT FIBER TYPES AND COMBINATIONS

Pitcha JONGVIVATSAKUL[*1], Koji MATSUMOTO[*2] and Junichiro NIWA[*3]

ABSTRACT

This paper aims to investigate the shear carried by fibers of fiber reinforced concrete (FRC) beams with different types and combinations of fibers. Eight FRC beams with five types and three combinations of fibers were tested. The results demonstrated that the stress across the diagonal crack and the angle of diagonal crack increased with the increase in fracture energy; in contrast, the diagonal crack length became shorter. The shear carried by fibers was investigated based on tension softening curves. Good correlation between tested results and calculated results was observed.

Keywords: steel fibers, synthetic fibers, hybrid fibers, shear carried by fibers, tension softening curves

1. INTRODUCTION

The addition of short discrete fibers into concrete is known to improve the post-cracking tensile strength and, hence, enhances the shear capacity of the structures. In the past three decades, most of the research works on fiber reinforced concrete (FRC) beams have been focused exclusively on steel fibers [1, 2]. However, some researchers [3, 4] examined the shear behavior of FRC beams with synthetic fibers. Nevertheless, these studies were performed with the limited kinds of fibers and without stirrups.

The Japanese design guidelines for steel fiber reinforced concrete piers [5] have recommended the equation for predicting the shear capacity of FRC beams with steel fibers. There is a lack of guidelines for design of FRC beams with various types of fibers. It is because the effectiveness of synthetic and hybrid fibers as shear reinforcements has not been clarified.

The main purpose of the test reported in this paper is to investigate the shear carried by fibers of FRC beams with different fiber types and combinations. The effectiveness of steel, synthetic and hybrid fibers as shear reinforcement is examined. The method to evaluate the shear carried by fibers using tension softening curves proposed in the previous study by the authors [6] is applied in this study. In the previous study [6], the proposed method accurately evaluated the shear carried by 30-mm steel fibers. However, it has not yet been extended to evaluate the shear carried by other types of fibers. In this study, eight FRC beams were tested. The stress transferred across the diagonal crack is calculated using the relationship between the tension softening curve and crack surface displacement. The shear carried by fibers is examined from the stress and the area of stress transferred. Finally, the calculated results are compared with the experimental results.

2. TEST PROGRAMS

2.1 Specimens

Eight FRC beams with different types of fibers were prepared. Five fiber types and three combinations of fibers were incorporated into concrete, including steel, synthetic and hybrid fibers. Table 1 lists the detail of tested specimens. The specimens were named according to types of fibers used in the beams. The total volume fraction of fibers (ρ_f) was equal to 1.0% of the full volume of the concrete in all specimens. Figure 1 shows the dimension and reinforcing bar arrangement of a FRC beam. The shear span (a) was 700 mm and the effective depth (d) was 250 mm. The ratio of shear span to the effective depth (a/d) was 2.8. The longitudinal reinforcement ratio (p_w) was 2.7%. All specimens were controlled such that they would fail in the left shear span by providing fewer stirrups in the left shear span as shown in Fig. 1. The stirrup ratio in the test span (r_w) was 0.30% in all specimens.

2.2 Materials

(1) Reinforcing materials

Properties of fibers are also shown in Table 1. Figure 2 presents the pictures of steel and synthetic fibers. In addition, two longitudinal reinforcing bars were made of deformed steel having 25.4-mm nominal diameter (D25). The stirrups made of deformed bars that had 6.35 mm in nominal diameter (D6) were arranged as the shear reinforcement. The yield strengths of these bars are listed in Table 1. Two round bars of 6-mm diameter (∅6) were used as compression bars.

(2) Concrete

Concrete used to prepare the beams was made from high-early strength Portland cement, fine aggregates, coarse aggregates and high-performance

*1 Ph. D. Candidate, Graduate School of Science and Engineering, Tokyo Institute of Technology, JCI Member
*2 Assistant Prof., Dept. of Civil Engineering, Tokyo Institute of Technology, Dr. E., JCI Member
*3 Prof., Dept. of Civil Engineering, Tokyo Institute of Technology, Dr. E., JCI Member

Table 1 Experimental cases

Beam	Material type of fiber	Fiber volume ρ_f (%)	Properties of fibers						p_w *4 (%)	f_y *5 (MPa)	r_w *6 (%)	f_{wy} *7 (MPa)	s *8 (mm)
			L_f *1 (mm)	D_f *2 (mm)	Density (kg/m^3)	Strength (MPa)	E *3 (GPa)	Shape of the end					
SF30	Steel	1.0	30	0.62	7850	1050	210	Hooked	2.7	1022	0.3	325	140
SF60	Steel		60	0.90	7850	1050	210	Hooked				315	
PP	Polypropylene		30	1.6×0.6	910	470	15	Straight					
PVA	Polyvinyl alcohol		30	0.66	1300	960	23	Straight					
PET	Polyethylene terephthalate		30	0.70	1370	460	5.8	Straight					
30-PP	SF30 and PP	0.5% and 0.5%	-	-	-	-	-	-		1012		328	
60-PP	SF60 and PP		-	-	-	-	-	-					
30-60	SF30 and SF60		-	-	-	-	-	-					

*1 fiber length, *2 diameter of fiber, *3 elastic modulus, *4 longitudinal reinforcement ratio, *5 yield strength of longitudinal reinforcement, *6 stirrup ratio, *7 yield strength of stirrups and *8 spacing of stirrups in test span.

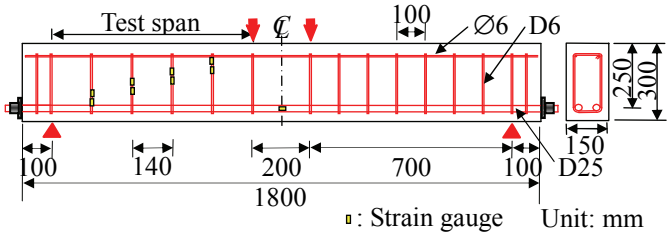

Fig. 1 Detailed diagram of a FRC beam

Table 2 Mixture proportion for concrete

G_{max} (mm)	W/C	Unit weight (kg/m^3)				
		W	C	S	G	SP
20	0.35	165	471	917	790	5.2

G_{max} = maximum size of the coarse aggregate, W = water, C = cement, S = fine aggregate, G = coarse aggregate, SP = high-performance air-entraining (AE) water-reducing agent

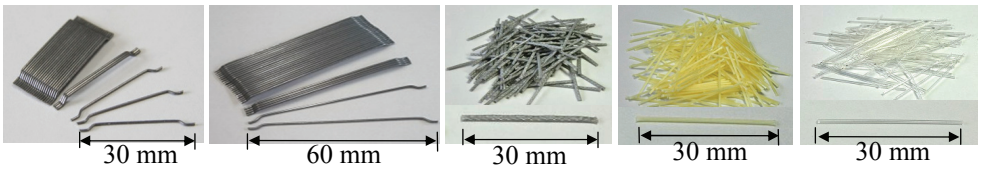

(a) SF30 (b) SF60 (c) PP (d) PVA (e) PET

Fig. 2 Steel and synthetic fibers

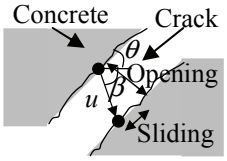

Fig. 3 Definition of u

air-entraining (AE) water-reducing agent. Table 2 shows the mixture proportion for concrete. The concrete was designed with the slump of 20±2.0 cm and an average 7-day age strength of 50 MPa.

2.3 Loading Method and Measurement Items

Specimens were subjected to a four-point bending with a simply-supported condition as illustrated in Fig. 1. Steel plates were placed on the pin-hinge supports and loading points.

The measuring items were the applied load, displacements at the mid-span and supporting points using transducers and the strain of the longitudinal reinforcing bars and stirrups. The strain of longitudinal steel bars was measured at mid span while the strains of stirrups were measured at the locations that diagonal crack was expected to occur as shown in Fig. 1. These stirrup strains are used for the calculation of the shear carried by stirrups. In addition, the crack surface displacement (u) and the angle of principal tensile strain (β) were measured from the image analysis system developed by Higashi et al. [7]. Crack surface displacement (u) is defined as the total displacement of cracks in the direction of principal tensile strain (β), which is the direction of the crack's movement as shown in Fig. 3. To analyze the image, red targets of 5-mm diameter were attached on the specimen surface with an interval of 20 mm. During the loading test, photographs of the specimens were captured for every 5 kN of shear force by using three digital cameras fixed on tripods. In addition, nearly the peak load, the photographs were captured with short time intervals to capture the exact behavior at the peak. The image analysis system can investigate the coordinates of the red targets throughout the test span. As a result, u and β can be calculated. Moreover, the length (L) and angle (θ) of the diagonal crack were measured from the visible diagonal crack at the peak load by using the software system, which supports analytical functions ranging from the image measurement to statistical data processing. The calibration was performed to define the length of one pixel in the image for converting the measurement data in pixels to actual lengths.

3. TENSION SOFTENING CURVES

The tension softening curves were used to investigate the stress transferred across the diagonal crack of FRC beams. The curves were obtained from the bending tests of notched beams with a dimension of

Table 3 Results of notched beam tests

Type	f'_c [*1] (MPa)	f_t [*2] (MPa)	G_F [*3] (N/mm)	Expressions of tension softening curves [*4]
SF30	56.6	3.6	4.24	$\sigma = \begin{cases} 7.0-40.2u & \text{for } u < 0.13 \text{ mm} \\ 1.85-0.55u & \text{for } u \geq 0.13 \text{ mm} \end{cases}$
SF60	55.9	3.4	8.82	$\sigma = \begin{cases} 4.3-50.5u & \text{for } u < 0.04 \text{ mm} \\ 2.3-0.31u & \text{for } u \geq 0.04 \text{ mm} \end{cases}$
PP	58.8	3.9	3.02	$\sigma = \begin{cases} 3.9-23.5u & \text{for } u < 0.12 \text{ mm} \\ 1.1-0.18u & \text{for } u \geq 0.12 \text{ mm} \end{cases}$
PVA	59.9	3.6	2.34	$\sigma = \begin{cases} 3.6-18.2u & \text{for } u < 0.16 \text{ mm} \\ 0.7-0.09u & \text{for } u \geq 0.16 \text{ mm} \end{cases}$
PET	61.5	3.3	2.89	$\sigma = \begin{cases} 3.4-25.2u & \text{for } u < 0.10 \text{ mm} \\ 0.9-0.25u & \text{for } u \geq 0.10 \text{ mm} \end{cases}$
30-PP	48.0	2.6	3.27	$\sigma = \begin{cases} 4.4-51.7u & \text{for } u < 0.06 \text{ mm} \\ 1.32-0.38u & \text{for } u \geq 0.06 \text{ mm} \end{cases}$
60-PP	44.5	2.6	7.49	$\sigma = \begin{cases} 3.7-17.4u & \text{for } u < 0.11 \text{ mm} \\ 1.82-0.26u & \text{for } u \geq 0.11 \text{ mm} \end{cases}$
30-60	44.9	2.4	7.50	$\sigma = \begin{cases} 5.3-41.2u & \text{for } u < 0.08 \text{ mm} \\ 2.03-0.35u & \text{for } u \geq 0.08 \text{ mm} \end{cases}$

[*1] compressive strength, [*2] tensile strength from split cylinder test [*3] fracture energy and [*4] formulated from the results of tension softening curves analyzed following the JCI standards [8].

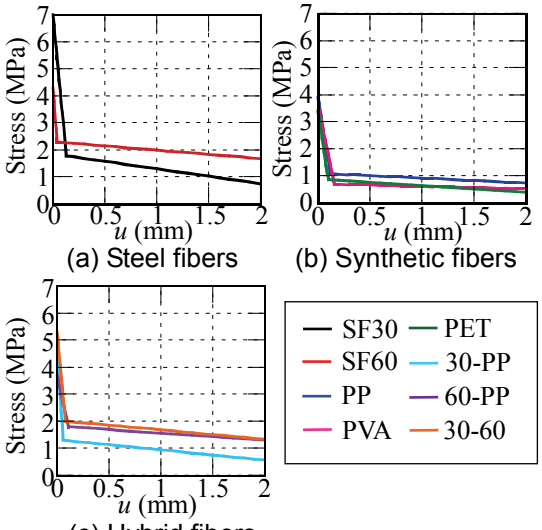

Fig. 4 Tension softening curves

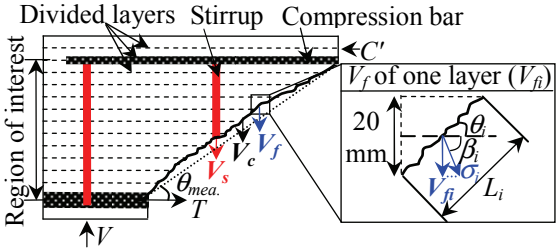

Fig. 5 Free body diagram of a FRC beam

100 × 100 × 400 mm following the standard of the Japan Concrete Institute [8]. The mixture proportion for concrete, the volume fraction and types of fibers used in the notched beams were same as those of FRC beams.

Table 3 lists the compressive strength, tensile strength and fracture energy (G_F) of the concrete measured by notched beam tests. G_F of SF60 was the highest among the all fiber types. The tension softening curves of eight types of fiber reinforced concrete are shown in Fig. 4 and the expressions are listed in Table 3. The results showed that SF30 revealed the highest peak stress. However, SF60 resisted the highest stress across the crack after $u \geq 0.12$ mm. It is because fiber length increased; thus, the bonding strength improved. At the identical crack opening displacement, steel fibers (SF30 and SF60) transferred higher stress than that by synthetic fibers (PP, PVA and PET) due to their high tensile strength and anchorage, while hybrid fibers showed the moderate stress. The stress transferred between crack surfaces was lost in two mechanisms. SF30, SF60, PP, 30-PP, 60-PP and 30-60 failed in the pull-out mechanism, whereas PVA and PET exhibited both pull-out and cut-off mechanisms. Because the tensile strength of fibers was comparatively greater than their bond strength, pull-out failure occurred.

4. CALCULATION OF SHEAR FORCES

By considering the free body diagram of a part of the shear span of a FRC beam subjected to point load (Fig. 5), the shear capacity (V) of FRC beams can be expressed as:

$$V = V_c + V_s + V_f \tag{1}$$

$$V_c = 0.2 \cdot \sqrt[3]{f'_c} \cdot \sqrt[4]{1000/d} \cdot \sqrt[3]{100\,p_w} \cdot b_w \cdot d \tag{2}$$

$$V_s = A_w f_{wy} (z \cot\theta / s) \tag{3}$$

where V_c is the shear capacity of members without stirrups (N), V_s is the shear carried by stirrups (N), V_f is the shear carried by fibers (N), f'_c is the compressive strength of the concrete (MPa), d is effective depth (mm), p_w is longitudinal reinforcement ratio, b_w is web thickness (mm), s is stirrup spacing (mm), A_w is the total cross-sectional area of stirrups provided in the range of s (mm^2), f_{wy} is the yield strength of stirrups (MPa), z is distance from the location of compressive stress resultant to the centroid of tension steel ($z = 7d/8$) (mm) and θ is the angle between the diagonal crack and horizontal line measured from the observed diagonal crack ($=\theta_{mea.}$) (degree).

The experimental value of shear carried by fibers (V_{fexp}) can be obtained from Eq. (4).

$$V_{fexp} = V_{exp} - V_c - V_s \tag{4}$$

Furthermore, according to the JSCE design guidelines [5], the shear capacity of FRC members can be predicted by using Eq. (5). Thus, the experimental value of $\kappa (= \kappa_{exp})$ can be calculated by Eq. (6).

Table 4 Summary of the calculation and experimental results of FRC beams

Beam	Concrete properties			Results of diagonal crack at the peak						Calculation and experimental results						
	f'_c [*1] (MPa)	f_t [*1] (MPa)	G_F [*2] (N/mm)	u [*3] (mm)	σ [*4] (MPa)	L [*5] (mm)	β [*6] (°)	θ [*7] (°)	$\theta_{mea.}$ [*8] (°)	V_{exp} (kN)	V_c (kN)	V_s (kN)	V_{fexp} (kN)	κ_{exp}	V_{fcal} [*9] (kN)	V_{fexp}/V_{fcal}
SF30	55.3	3.0	4.24	0.67	1.48	387.3	63.3	34.0	36.8	158.8	56.3	43.0	59.5	1.06	72.6	0.82
SF60	61.9	3.7	8.82	1.08	1.97	378.3	64.6	41.6	38.2	196.3	58.4	39.6	98.3	1.68	96.2	1.02
PP	57.0	3.1	3.02	0.94	0.93	428.1	69.2	32.2	27.5	170.8	56.9	59.8	54.1	0.95	53.6	1.01
PVA	65.4	3.0	2.34	0.69	0.64	490.6	63.7	27.8	27.0	166.8	59.5	61.1	46.1	0.78	40.4	1.14
PET	51.8	3.0	2.89	0.62	0.75	427.3	64.8	26.5	31.0	149.9	55.1	51.9	43.0	0.78	43.0	1.00
30-PP	52.2	2.7	3.27	0.59	1.09	388.1	61.9	34.8	33.0	151.2	55.2	50.0	46.1	0.83	55.0	0.84
60-PP	49.2	3.4	7.49	0.55	1.68	332.6	57.3	42.1	39.0	151.3	54.1	40.1	57.2	1.06	66.1	0.86
30-60	40.2	2.3	7.50	0.65	1.80	353.6	56.8	46.9	45.7	138.7	50.6	31.7	56.4	1.11	70.6	0.80

[*1] measured from specimens prepared together with FRC beams, [*2] fracture energy from notch beam tests, [*3] average crack surface displacement, [*4] average stress, [*5] total crack length, [*6] average angle of principal tensile strain, [*7] average angle of diagonal crack, [*8] measured angle between the diagonal crack and horizontal line and [*9] calculated shear carried by fibers based on tension softening curves (Eq. (7)).

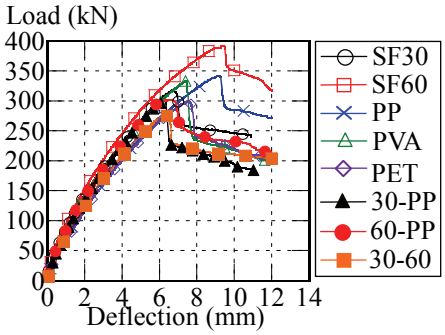

Fig. 6 Load-deflection curves

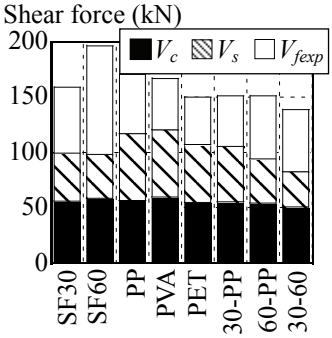

Fig. 7 V_c, V_s and V_{fexp} of FRC beams

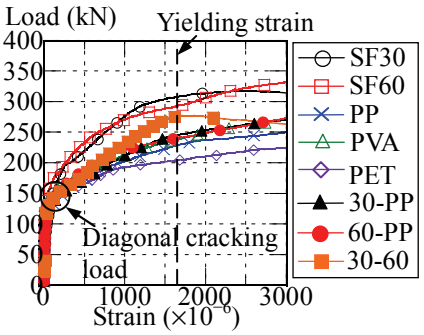

Fig. 8 Average stirrups strain

However, Eq. (5) was proposed only for steel fiber reinforced concrete members having 1.0–1.5% fiber of full concrete volume.

$$V_{JSCE} = (1+\kappa)\cdot V_c + V_s \quad (5)$$

$$\kappa_{exp} = V_{fexp} / V_c \quad (6)$$

where V_{JSCE} is the predicted shear capacity from JSCE equation and κ is the coefficient representing the effect of fibers (κ= 1.0).

5. RESULTS AND DISCUSSIONS

5.1 Load-Deflection Curves

Figure 6 presents the relationship between the applied load and the mid-span deflection. The load -deflection response exhibited the linear relation up to the first flexural crack. After the first flexural crack, the curve still increased linearly until the initiation of a diagonal crack in a shear span. Nonetheless, the formation of the diagonal crack did not mark the failure of FRC beams with stirrups and various fibers. The stirrups and fibers continued to carry the load until the crushing of concrete, which was the ultimate stage. Crushing was observed above the location of compression bars, where was in the compression zone. All tested beams failed in shear as indicated by the sudden drop in the load-deflection curves followed by a complete loss of load carrying capacity.

5.2 Effect of Fiber Types

Table 4 lists the concrete properties, information of diagonal cracks at the peak load, calculated and experimental results of shear forces. The values of V_c, V_s, V_{fexp} and κ_{exp} were calculated from Eqs. (2), (3), (4) and (6), respectively. The results show that SF60 revealed the highest shear capacity (V_{exp}) among all specimens. PP provided the highest V_{exp} among specimens with synthetic fibers. The value of V_{exp} of hybrid specimens was relatively low because the low f'_c in those beams. The shear contributions of concrete, stirrups and fibers are plotted in Fig. 7. V_c in each specimen was slightly different because of the difference of f'_c. On the other hand, V_s showed the variation due to the deviation from the angle between the diagonal crack and horizontal line ($\theta_{mea.}$). $\theta_{mea.}$ was measured as the angle between horizontal line and the linear line, which connected the points that the diagonal crack passed the locations of longitudinal bar and compression bar as shown in Fig. 5. The values of $\theta_{mea.}$ are given in Table 4. The specimens consisted of steel fibers (i.e. SF30, SF60, 30-PP, 60-PP and 30-60) provided steeper $\theta_{mea.}$ than synthetic fibers (PP, PVA and PET). As a result, V_s of specimens having steel fibers was lower than V_s of specimens having synthetic fibers. Figure 8 shows the average strain of stirrups in the test span. Stirrups in the test span were yielded before the ultimate load.

The experimental result of shear carried by

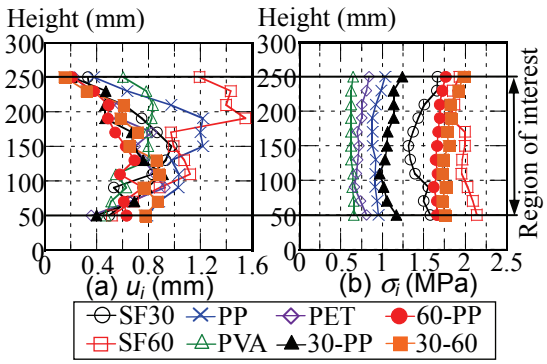

Fig. 9 Distributions of u_i and σ_i at peak load

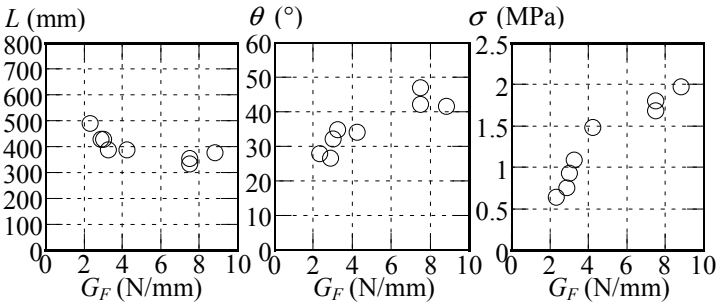

(a) Effect on L (b) Effect on θ (c) Effect on σ

Fig. 10 Effects of G_F on diagonal cracking behavior

fibers (V_{fexp}) of SF60 was the greatest as observed in Fig. 7, thereby resulting in the largest shear capacity. V_{fexp} increased with the increase in fiber length from 30 to 60 mm. In addition, the specimens including steel fibers showed higher V_{fexp} than synthetic fibers except 30-PP. Hybrid fibers were less effective. However, hybrid fibers with different fiber lengths (30 and 60 mm) were more effective than using the same length of fibers (only 30 mm). In case that enough anchorage and bond are provided, steel fibers are the most effective to enhance the shear carried by fibers.

The κ_{exp} of SF30, SF60, 60-PP and 30-60 were greater than 1.0, which is the value recommended in the design guidelines [5], whereas those of PP, PVA, PET and 30-PP were less than 1.0. By considering κ_{exp}, the shear contribution due to hybrid fibers was not dominant by one fiber type but it showed the average result between the two kinds of fibers that used as hybrid fiber.

5.3 Diagonal Cracking Behavior

In order to investigate the shear carried by fibers precisely, the specimens were divided into 15 layers. The information of diagonal crack of each layer (i.e. crack surface displacement (u_i), length of diagonal crack (L_i), angle of principal tensile strain (β_i) and angle of diagonal crack (θ_i)) (see Fig. 5) at the peak load were measured. The region of interest for investigation of the shear carried by fibers is the part between location of compression bars and tensile reinforcing bars (Fig. 5), where is 50-250 mm from the bottom of the specimens. The region of interest is where fibers show their tensile performance. The part above the location of compression bar is considered as the compression dominant zone because crushing of concrete happens in this portion. The shear carried by compression dominant zone is taken into account as a part of the shear carried by concrete (V_c). In addition, since the tip of the diagonal crack in tension zone stops at the location of tensile reinforcing bar, the height of tensile reinforcing bars is treated as the edge of the region of interest. The behavior of diagonal crack is discussed as follows:

(1) Crack surface displacement

The value of crack surface displacement of each layer (u_i) along the height of the diagonal crack at the peak load is shown in Fig. 9(a). u_i differed depending on the types of fibers. u_i at the peak load was in the parabolic shape and was varied in the range from 0.2 to 1.55 mm as observed in Fig. 9(a). The average values of u_i in the region of interest (u) are listed in Table 4. SF60 had the widest u among all specimens.

(2) Length of diagonal crack

The crack length (L) is the summation of crack length of each layer (L_i) in the region of interest. L is listed in Table 4. By varying types and combinations of fibers, there was a relation between L and G_F. L decreased with the increase in G_F as shown in Fig. 10(a). This tendency conforms to the effects of r_w and ρ_f on L as reported in the previous study [6]. This implies that G_F can be one of the indicators for the efficiency of fibers as a shear reinforcement.

(3) Angle of diagonal crack and angle of principal tensile strain

The angles of diagonal crack (θ_i) and principal tensile strain (β_i) of each layer were measured. The average values of θ_i and β_i in the region of interest (θ and β, respectively) are given in Table 4. θ was varied from 26.5° to 46.9°. The specimens with higher G_F tended to have steeper θ than those of low G_F as presented in Fig. 10(b). In contrast, β did not change significantly among these specimens.

6. INVESTIGATION OF SHEAR CARRIED BY FIBERS

6.1 Review of the Evaluation Method

A method for evaluating the shear carried by steel fibers by using tension softening curves was proposed by the authors [6]. By considering the force acting at the diagonal crack in a FRC beam due to the effect of fibers (Fig. 5), the shear carried by fibers (V_{fcal}) is the summation of forces in the region of interest, where is height of 50-250 mm from the bottom of specimen, and can be calculated from Eq. (7).

$$V_{fcal} = \sum_{i=1}^{n} \left(\sigma_i \cdot b_w \cdot L_i \cdot \cos\left(\beta_i + \theta_i - 90\right) \cdot \sin\beta_i \right) \quad (7)$$

where n is the number of layers in the region of interest (n = 11), σ_i is the tensile stress of the layer i (MPa), L_i is the length of the diagonal crack of the layer i (mm), β_i is the angle of the principal tensile strain of layer i (degree) and θ_i is the angle of the diagonal crack of the

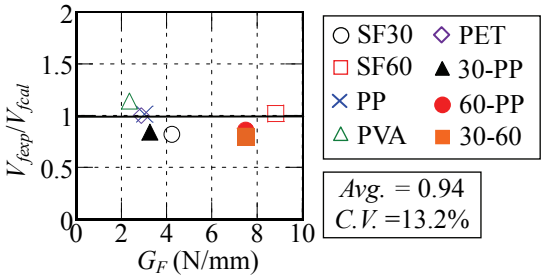

Fig. 11 Comparison between V_{fexp} and V_{fcal}

layer i (degree).

6.2 Calculated Shear Carried by Fibers

The values of u_i were converted to the tensile stress transferred across the diagonal crack (σ_i) at the peak load by using the relationship of tension softening curves (that is the expressions in Table 3). The distribution of σ_i is shown in Fig. 9(b). Although u_i of the specimens was varied without the clear tendency, the value of σ_i was significantly different and a tendency was observed. It is because each fiber reinforced concrete transferred the different stress at the identical crack surface displacement as observed in tension softening curves. SF60 resisted the highest σ_i resulting in the largest V_{fexp}. Synthetic fibers resisted relatively low and uniform σ_i at the peak load due to their flat slope of the second branch of tension softening curves (i.e. when $u \geq 0.12$, 0.10 and 0.16 mm for PP, PVA and PET, respectively). Hybrid fibers containing SF60 provided high σ_i at the peak load because of the influence of the long fibers. The average value of σ_i in the region of interest (σ) is listed in Table 4. σ increased with the increase in G_F as observed in Fig. 10(c).

In addition, the area of crack surface was calculated from b_w, L_i, β_i and θ_i. The area of crack surface, which is the area of crack that is perpendicular to the direction of principal stress σ_i, is equal to $b_w \cdot L_i \cdot \cos(\beta_i + \theta_i - 90)$ as presented in Eq. (7). The area of crack surface was mainly affected by L_i and θ_i because b_w and β_i were not varied. The shear carried by the fibers (V_{fcal}) was calculated using Eq. (7) and is summarized in Table 4. Although the stress of hybrid fibers was high, the area of crack surface was small due to the short L_i and steep θ_i. Thus, the shear carried by fibers did not increase significantly. Figure 11 shows the ratio between the experimental results and calculated values (V_{fexp}/V_{fcal}) versus G_F. The mean of V_{fexp}/V_{fcal} was 0.94 with a coefficient of variation ($C.V.$) of 13.2%. Good agreement between experimental results and calculated results was observed. The proposed method can evaluate the shear carried by fibers with good accuracy even though types and combinations of fibers are varied.

7. CONCLUSIONS

(1) Steel fibers are the most effective to increase the shear carried by fibers than synthetic and hybrid fibers when there is enough fiber length and bonding strength. In case of hybrid fibers, the combinations between different fiber lengths are more effective than that of the same fiber length.

(2) The fracture energy affects the diagonal cracking behavior of fiber reinforced concrete beams. The stress across the diagonal crack and the angle of diagonal crack increase with the increase in fracture energy; on the other hand, the diagonal crack length decreases. However, the angle of principal tensile strain did not change significantly in the range of this study.

(3) Although types and combination of fibers were varied, the calculated shear carried by fibers showed good agreement with the experimental values. The proposed method can be used to investigate the shear carried by fibers regardless of the types and combination of fibers.

ACKNOWLEDGEMENT

The authors wish to acknowledge the supports of the Center for Urban Earthquake Engineering (CUEE) of Tokyo Institute of Technology.

REFERENCES

[1] Narayanan, R., and Darwish, I. Y. S., "Use of Steel Fibers as Shear Reinforcements," ACI Structural Journal, ACI, Vol. 84, No. 3, May-June 1987, pp. 216-227.

[2] Kwak, Y.-K., Eberhard, M. O., Kim, W.-S., and Kim, J., "Shear Strength of Steel Fiber-Reinforced Concrete Beams without Stirrups," ACI Structural Journal, ACI, Vol. 96, No. 4, Jul. 2002, pp. 530-538.

[3] Li, V. C., Ward, R., and Hamaza, A. M., "Steel and Synthetic Fibers as Shear Reinforcement," ACI Materials Journal, ACI, Vol. 89, No. 5, Sept.-Oct. 1992, pp. 499-508.

[4] Altoubat, S., Yazdanbakhsh, A., and Rieder, K. A., "Shear Behavior of Macro-Synthetic Fiber-Reinforced Concrete Beams without Stirrups," ACI Materials Journal, ACI, Vol. 106, No. 4, Jul.-Aug. 2009, pp. 381-389.

[5] JSCE, "Guidelines of Design for RSF Piers," Concrete Library 97, 1999, p. 15. (in Japanese)

[6] Jongvivatsakul, P., Watanabe, K., Matsumoto, K., and Niwa, J., "Evaluation of Shear Carried by Steel Fibers of Reinforced Concrete Beams Using Tension Softening Curves," Journal of Materials, Concrete Structures and Pavements, JSCE, Vol. 67, No. 4, Oct. 2011, pp. 493-507.

[7] Higashi, H., Watanabe, K., and Niwa, J., "Image Analysis for Failure Mode of RC Beams with Fractured Longitudinal Reinforcement," Proceedings of the JCI, Vol. 31, No. 2, Jul. 2009, pp. 727-732. (in Japanese)

[8] JCI, "Method of Test for Fracture Energy of Concrete by Use of Notched Beams," Japan Concrete Institute Standard, 2003.